

Giant isoscalar monopole resonance strength in ^{40}Ca from $(e, e' \alpha)$ angular correlations

M. Kohl, P. von Neumann-Cosel, A. Richter, G. Schrieder, and S. Strauch
Institut für Kernphysik, Technische Universität Darmstadt, D-64289 Darmstadt, Germany
 (Received 9 February 1998)

The giant resonance region in ^{40}Ca has been studied with inelastic electron scattering at the Mainz microtron MAMI and the superconducting Darmstadt linear accelerator S-DALINAC for a momentum transfer range $q = 0.25 - 0.66 \text{ fm}^{-1}$. Complete angular correlation functions for the coincident α decay into the ground state (α_0) and first excited state (α_1) of ^{36}Ar have been measured. A model-independent multipole decomposition is presented for the α_0 channel under the assumption of a mixture of $E0/E1/E2$ strengths. It is demonstrated that this method can be extended to the α_1 channel assuming that the relative weight of the allowed decay angular momenta is determined by transmission coefficients and for a specific choice of relative phases between multipole amplitudes suggested by the data. The resulting distributions of isoscalar $E0$ and $E2$ strengths for the α_0 and α_1 channels are tested against microscopic calculations including coupling to the continuum and complex configurations of the $1p-1h \otimes$ phonon type. Assuming statistical decay the total isoscalar $E0$ response can be reconstructed. An exhaustion of 44.2(8.8)% of the energy-weighted sum rule for the isoscalar giant monopole resonance is found in the excitation energy interval 11–19 MeV. The $B(E0)$ strength distribution is in fair agreement with recent (α, α') measurements under extreme forward angles suggesting a centroid energy of about 17–18 MeV. [S0556-2813(98)02906-9]

PACS number(s): 25.30.Fj, 24.30.Cz, 23.20.Js, 27.40.+z

I. INTRODUCTION

Among the giant resonances the isoscalar giant monopole resonance (GMR) plays a special role because it provides a measure of a fundamental quantity of nuclear matter—the compressibility. The relation is usually expressed by the nuclear matter compression modulus K_{nm} which is a function of the frequency of the mode and the moments of its energy distribution [1]. The compressibility exhibits a strong mass dependence. Thus, experimental information on the GMR from a wide range of nuclei is important. The GMR has been established in heavy nuclei ($A \geq 90$) where it forms a compact resonance with a Lorentzian shape (see [2], and references therein). However, in light nuclei the isoscalar $E0$ strength was found to be very fragmented and only in a few cases a significant fraction of the energy-weighted sum rule (EWSR) has been detected [3,4].

Recently a controversy arose on the value of K_{nm} which can be extracted from the data. Based on microscopic calculations [1,5,6] $K_{\text{nm}} \approx 210(30) \text{ MeV}$ was generally accepted. However, Sharma *et al.* [7] claimed a much higher value $K_{\text{nm}} = 300(20) \text{ MeV}$. Their analysis, based on an approach similar to the semiempirical mass formula, was questioned by Pearson [8] and Shlomo and Youngblood [9]. On the other hand, calculations within the relativistic mean-field theory [10,11] using density-dependent interactions with nuclear matter compressibilities varying approximately between $K_{\text{nm}} \approx 200$ and 600 obtain the best description of the GMR energy in heavy nuclei for values between 250 and 270.

While the predictions of different models [6,10–13] tend to agree for heavier nuclei, differences are more pronounced for nuclei with smaller mass numbers. Thus, to shed light on this problem further experimental information on the GMR in light and medium-mass ($A \leq 70$) nuclei would be helpful. The most successful experimental approach [2] to study the

GMR is inelastic α scattering at extreme forward angles because of its selectivity to isoscalar excitations and the dominance of the monopole cross section at angles close to 0° . Recently, results have become available from the Texas A&M group for ^{58}Ni [14] and ^{40}Ca [15] obtained with an improved experimental setup allowing for excellent peak-to-background ratios and studying a wide excitation energy range up to 30 MeV. Surprisingly, the experimental findings differ appreciably. While an exhaustion of less than 50% of the EWSR is found in ^{58}Ni , close to 100% is extracted for ^{40}Ca . However, the latter value contains a large contribution from a multipole analysis of the background underlying the resonance structure which has considerable ambiguities in the fit to the data [15].

Theoretically, such a large difference in the fragmentation of the GMR strength for nuclei reasonably close in mass number and studied under comparable experimental conditions is hard to understand in microscopic models [16]. There is a basic uncertainty of all giant resonance studies with hadronic probes with respect to the conversion of measured cross sections to transition strengths. It depends on the optical potentials which can be derived with different assumptions about the interaction (deformed potential, single, and double folding etc.), and for the monopole case also on the assumed form of the transition density, where typically the breathing mode of Satchler [17] is used. The impact of different choices on the resulting exhaustion of the isoscalar $E0$ EWSR can be quite large (see, e.g., [18,19]).

Electron-scattering coincidence experiments provide a potentially very attractive alternative for the investigation of the GMR not hampered by the limitations described above. Experimental studies of giant resonances with this method [20–29], which have become possible with a new generation of continuous-wave electron accelerators, should provide the most reliable information on the transition strengths because the response of the nucleus is measured essentially

background free and the nature of reactions with electromagnetic probes is well understood. However, investigations of the GMR in medium-mass nuclei, where it strongly overlaps with the isoscalar giant quadrupole resonance (GQR), are limited by the similarity of the $E0$ and $E2$ form factors in electron scattering. Nevertheless, a separation of the different multipolarities can be achieved from measurements of the angular correlations of the decay particles populating resolved final states. This method has been successfully applied, e.g., to $(e, e' \alpha)$ reactions in ^{12}C , ^{16}O , and ^{26}Mg for the decay to the $J^\pi = 0^+$ ground state of the daughter nucleus [25–27]. For nucleon (proton or neutron) decay, unless for the particularly simple case of one dominating multipole [20,30], a model-independent analysis is not possible, and information can only be extracted from the comparison to model calculations [28,29].

The present work reports an investigation of the GMR strength in ^{40}Ca with the $(e, e' \alpha)$ reaction to resolved final states for excitation energies up to 20 MeV. It is clear that only a fraction of the total isoscalar $E0$ strength present in this energy range is extracted, but in nuclei where it is reasonable to assume statistical decay of the GMR—which seems to be the case [28,31] in ^{40}Ca —the total strength can be reconstructed. The analysis of giant multipole strength in ^{40}Ca is complicated by the presence of three overlapping resonances: the GMR, the GQR and the isovector giant dipole resonance (GDR) which contribute with comparable magnitude to the electron-scattering cross sections. However, it has been shown by Ref. [32] that an analytical decomposition of angular correlation of the $(e, e' \alpha)$ reaction leading to the ground state (g.s.) of the daughter nucleus (α_0 channel) is still possible for three multipolarities. Such an analysis has been presented for the $^{40}\text{Ca}(e, e' \alpha_0)^{36}\text{Ar}_{\text{g.s.}}$ reaction in [33] which provided clear evidence for the presence of appreciable amounts of low-energy isoscalar $E0$ and $E2$ strength in contrast to random-phase approximation (RPA) predictions. This shift of strength to low energies can be traced back to g.s. correlations allowing for $0\hbar\omega$ transitions forbidden in the independent particle model [34]. Here, we give a full account of the results and furthermore show that an extension of the method proposed in [32] is possible for the decay into the first excited $J^\pi = 2^+$ state in ^{36}Ar (α_1 channel) with the additional assumptions that the weight of the different decay angular momenta of a given resonance is determined by transmission coefficients and for a particular choice of phases between the various multipole amplitudes suggested by the data.

The experiments are described in Sec. II, while Sec. III presents the basic ideas of the angular correlation analysis. The resulting $E0$ strength distributions are discussed in Sec. IV, and concluding remarks are given in Sec. V. The mathematical details of the angular correlation analysis are presented in the Appendix.

II. EXPERIMENTS

The experiments were performed at the Mainz microtron MAMI A at an incident energy $E_0 = 183.5$ MeV and three scattering angles $\theta_e = 22.0^\circ$, 31.4° , and 43.0° corresponding to momentum transfers $q = 0.35$, 0.49 , and 0.66 fm $^{-1}$, respectively. Further data were taken at the superconducting

Darmstadt electron linear accelerator S-DALINAC at a lower q of 0.25 fm $^{-1}$ (with $E_0 = 78$ MeV and $\theta_e = 40.0^\circ$). Self-supporting natural calcium foils of about 1 mg/cm 2 were used as targets. Typical electron currents were 10 μA at MAMI and up to 5 μA at the S-DALINAC. The scattered electrons were detected by a 180° double-focusing magnetic spectrometer with a solid angle of 4 msr in the Mainz experiment [35] and with a QCLAM magnetic spectrometer subtending 34 msr solid angle [28] in Darmstadt. The decay of charged particles was measured with up to 10 particle telescopes consisting of a 75 – 100 μm ΔE and 1 mm E silicon counter backed by a second 1 mm detector used as anticoincidence. The telescopes were placed on a goniometer out of plane at an azimuthal angle $\Phi_\alpha = 135^\circ$ (in the convention of [36]). Data were typically taken for emission angles $\theta_\alpha = 0^\circ$ – 230° in 10° steps, where θ_α is defined with respect to the momentum transfer axis.

In the excitation range in ^{40}Ca considered here ($E_x \approx 10$ – 20 MeV) only proton and α emission contribute to the charged particle decay. The target thickness was limited such that losses of the α particle flux due to straggling could be avoided. Thus, the low-energy threshold of α particle spectra was always determined by the Coulomb barrier. The detector thicknesses were chosen for easy distinction of proton and α particles, since the latter were always stopped in the first counter. For low energy protons, which could not traverse the ΔE detector, separation was achieved by a time-of-flight technique. It utilized the range-dependent charge collection times when the ΔE detectors are mounted reverse to the normal operation mode.

The ability to resolve specific final states in the $(e, e' x; x = p, \alpha)$ reaction is limited by the energy straggling in the target which amounts to typical values of about 250 keV for the protons and 700 keV for the α particles; the resolution of the electron spectra of about 120 keV in Mainz and 50 – 70 keV in Darmstadt can be neglected. The level scheme of ^{36}Ar populated in the $^{40}\text{Ca}(e, e' \alpha)$ reaction thus allows us to extract angular correlations for decay to the g.s. and the first excited state at 1.98 MeV. The top part of Fig. 1 presents the excitation energy spectrum of ^{40}Ca measured at $E_0 = 183.5$ MeV, $\theta_e = 31.4^\circ$ and extracted under the condition of coincident emission of an α particle. Below, a separation into the parts corresponding to the coincident α_0 and α_1 decays and the remaining contribution due to decay into higher-lying states in ^{36}Ar (α_{Rest}) is presented. The population ratio is largely independent of the momentum transfer because $E0$ and $E2$ excitations dominate which exhibit roughly the same q dependence. Contributions of the GDR are very small in the α decay because of isospin selection rules. The centroids of the separated cross section parts in Fig. 1 rise from $E_x \approx 14$ MeV for coincident α_0 emission to $E_x \approx 16$ MeV for α_1 and $E_x > 18$ MeV for α_{Rest} . The cross sections are comparable for all three channels, but one should keep in mind that α decay represents only a rather small fraction of the total $^{40}\text{Ca}(e, e' x)$ cross section (approximately 10 – 35 % in the measured momentum transfer range). The overall error of the cross sections is estimated to be less than ± 20 % in all cases, including statistics (≤ 10 %), uncertainty of the target thickness (≤ 10 %), charge collection (≤ 5 – 10 %), and geometrical uncertainties (≤ 2 %).

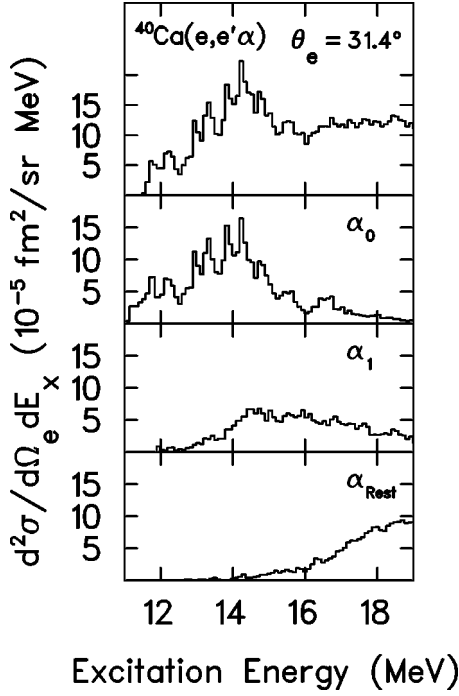


FIG. 1. Excitation spectrum of the $^{40}\text{Ca}(e,e'\alpha)$ reaction at $E_0 = 183.5$ MeV, $\theta_e = 31.4^\circ$ coincident with emission of an α particle and integrated over the α emission angle, and decomposition into the parts populating the g.s. (α_0), the first excited state (α_1) and higher-lying states (α_{Rest}) of ^{36}Ar , respectively.

Angular correlations for the α_0 and α_1 reaction channels have been measured at angles Θ_α relative to the axis defined by the momentum transfer q imparted onto ^{40}Ca by the electron. Typical examples are depicted for $E_0 = 183.5$ MeV and $\theta_e = 43.0^\circ$ in Figs. 2 and 3, respectively. The ^{40}Ca energy bins have been chosen to roughly follow prominent structures in the excitation spectrum. The solid lines are fits with a Legendre polynomial up to fourth order. All angular correlations show strong maxima at $\Theta_\alpha = 0^\circ$ and 180° and a weaker one at 90° . The shapes are reminiscent of $L=2$ decay, but pronounced differences of the maximum cross sections are observed between 0° and 180° indicating admixture of an odd angular momentum component (e.g., $L=1$). In Figs. 2 and 3 a systematic difference between the α_0 and α_1 channels can be clearly seen. While the largest cross section in the $(e,e'\alpha_0)$ angular correlation is always found at angles around $\Theta_\alpha \approx 0^\circ$, it is just the reverse for $(e,e'\alpha_1)$, where it is peaked at $\Theta_\alpha \approx 180^\circ$. This feature is also present in all angular correlations of α decay measured at the other momentum transfers.

III. ANALYSIS OF $(e,e'\alpha)$ ANGULAR CORRELATIONS

A. Model-independent method

The general form of the electron cross section with an α particle detected in coincidence can be expressed as the Mott cross section σ_{Mott} times bilinear products of kinematic factors V and corresponding structure functions W describing the nuclear dynamics [36]. Explicitly,

$$\frac{d^3\sigma}{d\Omega_e d\omega d\Omega_\alpha} = \sigma_{\text{Mott}}(V_L W_L + V_T W_T + V_{LT} W_{LT} \sin\Phi_\alpha$$

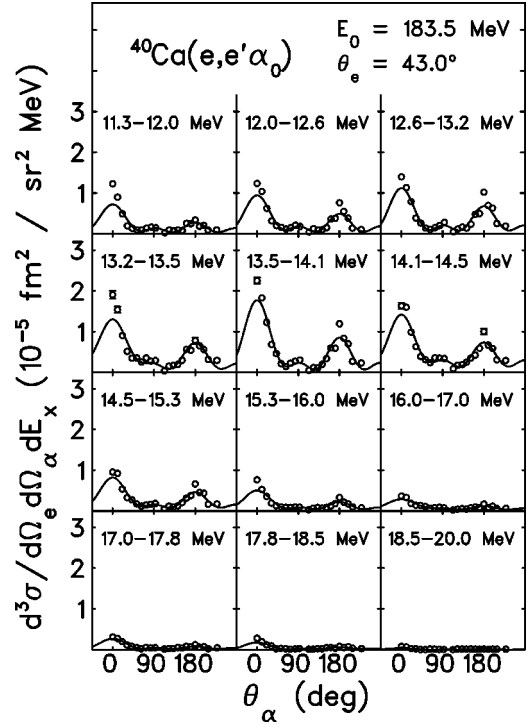


FIG. 2. Angular correlations of the $^{40}\text{Ca}(e,e'\alpha_0)$ reaction at $E_0 = 183.5$ MeV, $\theta_e = 43.0^\circ$ in the excitation energy range $E_x = 11 - 20$ MeV.

$$+ V_{TT} W_{TT} \cos 2\Phi_\alpha), \quad (1)$$

where the indices L , T , LT , and TT refer to the interaction of the exchanged virtual photon with the longitudinal and transverse currents in the nucleus, and the interference terms, re-

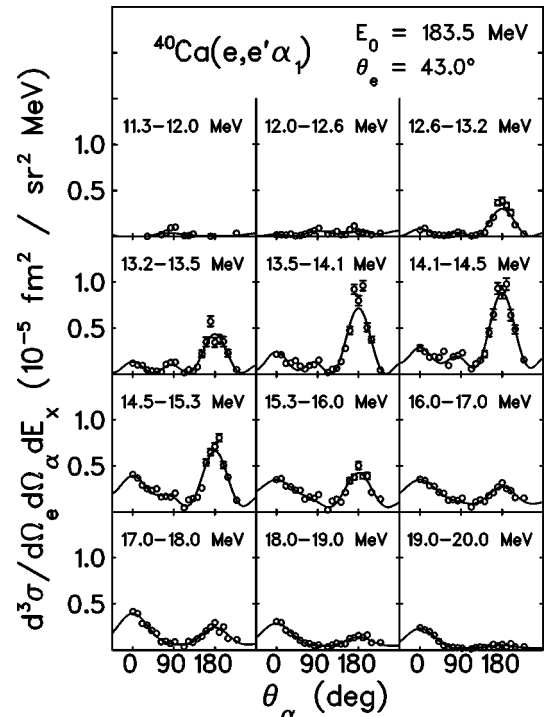


FIG. 3. Angular correlations of the $^{40}\text{Ca}(e,e'\alpha_1)$ reaction at $E_0 = 183.5$ MeV, $\theta_e = 43.0^\circ$ in the excitation energy range $E_x = 11 - 20$ MeV.

spectively. The structure functions can be expanded in multipoles using Legendre polynomials for L and T , and first- and second-order associated Legendre polynomials for LT and TT , respectively.

For the present experiment the TT interference term vanishes exactly because the angle Φ_α was chosen to be 135° . The LT interference term mainly results in a rotation of the symmetry axis which for the present data is generally smaller than 2° and can thus be neglected [37,38]. Applying Siegert's theorem one can estimate the transverse part of the cross section in the chosen kinematics to be less than 5% of the total cross section (less than 10% for the S-DALINAC measurement), and it can thus also be neglected. The three-fold differential cross section is therefore assumed to be purely longitudinal and is proportional to an angular correlation function (ACF) called W

$$\frac{d^3\sigma}{d\Omega_e dE_x d\Omega_\alpha} \propto W(\theta_\alpha) = \sum_l A_l P_l(\cos\theta_\alpha). \quad (2)$$

In the static limit of resonance approximation [36] for the case of $J^\pi=0^+$ targets the angular correlation coefficients can be written as

$$A_l = \sum_{S, LL', JJ'} A'_l(S; LJ; L' J') (C_{LJ}^{(S)} e^{i\delta_{LJ}^{(S)}})^* (C_{L'J'}^{(S)} e^{i\delta_{L'J'}^{(S)}}). \quad (3)$$

The factors A'_l contain the information of angular momentum coupling and are described in the Appendix. The quantity $C_{LJ}^{(S)} e^{i\delta_{LJ}^{(S)}}$ is the complex amplitude of the product between the longitudinal matrix element and the overlap of the intermediate resonance J and the decay channel (LS). For $J^\pi=0^+$ targets, the multipolarity of the excitation is identical with the angular momentum J of the resonance. The quantity L is identified with the relative orbital angular momentum of the emitted particle with respect to the remaining nucleus, and S represents the total spin of the final state determined by the particle spin and state of the residual nucleus. The expansion parameter l can be understood as the angular momentum resulting from the coupling of two interfering resonances J, J' . Because the α particle has spin zero, the decay to the ground state of ^{36}Ar ($J^\pi=0^+$) gives $S=0$ (α_0 channel), whereas the first excited state of ^{36}Ar ($J^\pi=2^+$) yields $S=2$.

Because of the low experimental momentum transfers q , contributions due to the excitation of $E3$ or higher multipole strength should be small [28]. Thus, the expansion in Eq. (2) is restricted to $l=4$, i.e., only $E0$, $E1$, and $E2$ transitions are assumed in the description of the ACF. Due to $S=0$ in the α_0 channel, only one partial wave occurs for each resonance ($J=L$). In the α_1 channel, however, the situation becomes more complicated. Applying parity selection rules, one obtains various (LJ) combinations in the α_1 channel as shown in Table I.

The ACF expansion up to $l=4$ gives five angular correlation coefficients A_l determined by a fit to the experimental data. Choosing one overall phase arbitrarily, there are three amplitudes and two phases left undetermined in the α_0 channel, which can be related to the five parameters A_l . While

TABLE I. Possible orbital angular momenta L and total spins S in the exit channel of the α decay of a resonance with spin J into the $J^\pi=0^+$ g.s. (α_0) or the $J^\pi=2^+$ first excited state (α_1) of the daughter nucleus.

Channel	J	S	L
α_0	0		0
	1	0	1
	2		2
α_1	0		2
	1	2	1,3
	2		0,2,4

the multipole decomposition based on Eq. (2) is unique for the highest multipolarity $E2$, there are three mathematically equivalent solutions for $E0$, $E1$ and the two relative phases, respectively. As already noted in [32] one solution is never realized by physical data, whereas the two other solutions are characterized by either a large or a small $E0/E1$ ratio, respectively. Physical arguments (isospin forbiddance of α decay from the GDR to isospin $T=0$ states in ^{36}Ar , q dependence of the form factors, and comparison to other work as discussed below) favor the solution with a large $E0/E1$ ratio.

B. Additional assumptions for the α_1 channel

The various LJ combinations in the α_1 channel (see Table I) lead to six additional parameters which cannot be uniquely determined by the data. One has to introduce model assumptions to fix them in order to be able to proceed with the analysis in analogy to the α_0 case.

The first assumption is as follows. The decay of an excited resonance of total angular momentum J shows branchings into all decay channels allowed by conservation of the orbital angular momentum L . Their relative magnitude is assumed to be determined by the transmission coefficients T_L . This can be expressed as

$$C_{LJ}^2 = \beta_L C_J^2, \quad \text{with } \beta_L = \frac{T_L}{\sum_{\text{allowed } L} T_L}. \quad (4)$$

The transmission coefficients are determined for the reaction $^{40}\text{Ca} \rightleftharpoons ^{36}\text{Ar} + \alpha$ and are calculated by the program code CASCADE [39] as a function of excitation energy taking the standard optical potential parameter set for the system $\alpha + ^{36}\text{Ar}$. Restricting J to values of 0,1,2 (as for the α_0 case) three parameters are fixed.

Furthermore, there are three phases to be determined. Considering the relative phases $\delta_{LJ} - \delta_{L'J}$, i.e., the modification of the phase of a resonance with spin J due to different decay channels L, L' there are two possible extremes. For a value of zero, the partial waves L, L' interfere totally constructively, whereas a totally destructive interference is achieved by the choice

$$e^{i(\delta_{LJ} - \delta_{L'J})} = i^{(L-L')}. \quad (5)$$

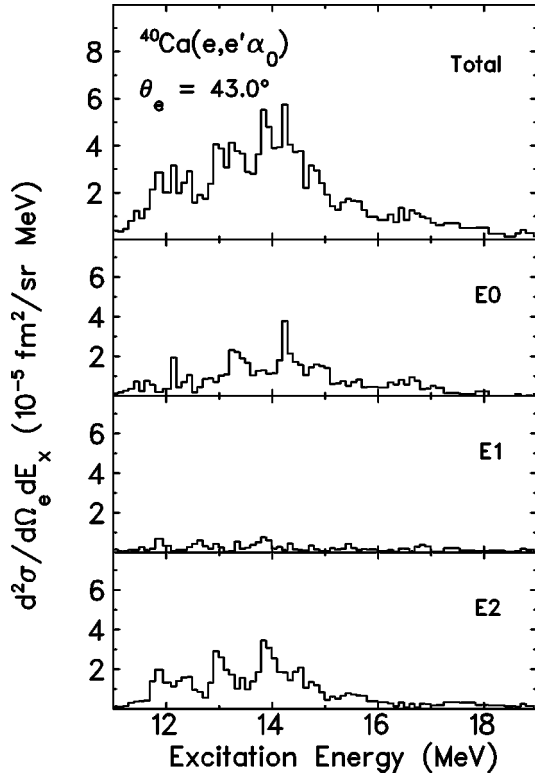


FIG. 4. Cross section of the $^{40}\text{Ca}(e, e' \alpha_0)$ reaction at $E_0 = 183.5$ MeV, $\theta_e = 43.0^\circ$ and its decomposition into $E0$, $E1$, and $E2$ parts using the method described in the Appendix.

Two neighboring L channels for a fixed J (which differ by $\Delta L = 2$ because of parity conservation), would thus be characterized by $e^{i(\delta_{LJ} - \delta_{L'J})} = -1$ resulting in a phase difference of 180° .

Detailed tests show that the first choice (constructive interference) yields only nonphysical solutions for the C_J^2 's in the whole excitation energy range, i.e., the solution for at least one C_J^2 always becomes negative. Only the second alternative (destructive interference) leads to physically possible values of the C_J^2 amplitudes. It is pointed out that with the assumption of Eq. (5) the structure of the system of equations [Eq. (A8)] described in the Appendix becomes exactly the same as for the α_0 channel [Eq. (A3)]. The only difference is a reversal of the signs of A_1 and A_3 , respectively. The coefficients A_1 and A_3 measure the interference of the $E0/E1$ and $E1/E2$ resonances, which result in an asymmetry of the angular distribution with respect to 90° . Such a systematic change of the signs, going from α_0 to α_1 , is clearly supported by the data for the whole excitation energy range investigated (see Figs. 2, 3).

C. Results

For the decomposition of the multipole parts, the angular correlations of the $^{40}\text{Ca}(e, e' \alpha_{0,1})$ reactions have been analyzed for energy bins of 100 keV in a ^{40}Ca excitation range $E_x = 11 - 19$ MeV. At higher energies the experimental cross sections become too small. Figures 4 and 5 display as examples the total and the decomposed $E0/E1/E2$ cross sections for the α_0 channel measured at $E_0 = 183.5$ MeV, $\theta_e = 43.0^\circ$ and for the α_1 channel at $E_0 = 183.5$ MeV, θ_e

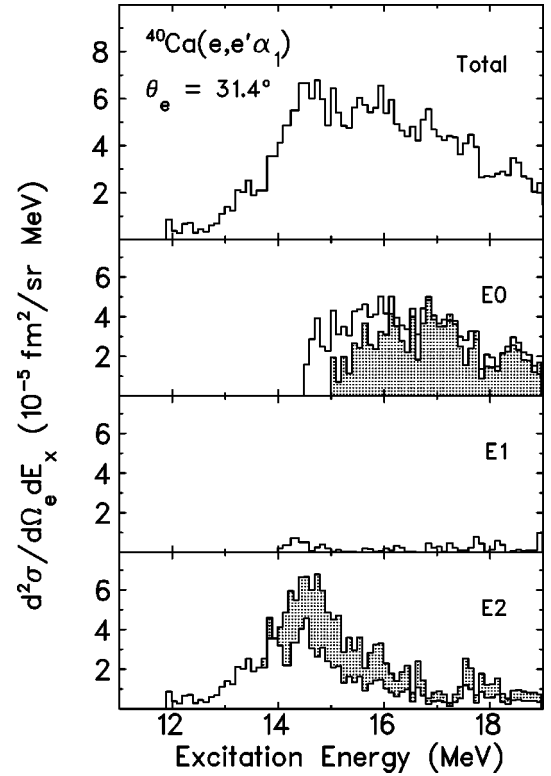


FIG. 5. Cross section of the $^{40}\text{Ca}(e, e' \alpha_1)$ reaction at $E_0 = 183.5$ MeV, $\theta_e = 31.4^\circ$, and its decomposition into $E0$, $E1$, and $E2$ parts using the method described in the Appendix. The open histograms correspond to relative phases of 180° and the hatched histograms to 0° between the amplitudes for a given resonance spin J and neighboring ($\Delta L = 2$) decay angular momenta L .

$= 31.4^\circ$. In both cases the $E0$ and $E2$ cross sections are of comparable magnitude while the $E1$ cross sections are a factor of about 10 smaller. The parts corresponding to the different multipolarities exhibit considerable fine structure in the α_0 decay for excitation energies up to 15 MeV. The predominance of $E2$ cross sections at the energies below 14 MeV in the α_1 decay reflects the possible decay angular momenta. While $E0$ strength requires $L = 2$ decay, $L = 0$ is also possible for $E2$ strength and dominates the region close to the threshold.

As discussed in Sec. III A the $E0/E1/E2$ decomposition is unique for the α_0 channel (except for the unphysical solution) whereas the analysis in the α_1 channel depends on the assumption of the relation between the relative phases of decay angular momenta expressed in Eq. (5). For the case of $E2$ strength its influence can be estimated. The hatched area in Fig. 5 shows the cross section resulting for phase differences equal to zero which represents an upper limit for the $E2$ contribution. As pointed out above no meaningful solutions are obtained for $E0$ and $E1$ with this assumption, but to illustrate the effects the additional cross section found in the $E2$ part is subtracted from $E0$. The result, which represents the minimum cross section due to $E0$ excitations, is again shown as hatched area in the corresponding part of Fig. 5. The main effect is at the lowest energies where the population is governed by the difference of the transmission coefficients for the possible angular momenta. The total effect of different phase relations on the multipole decomposition is

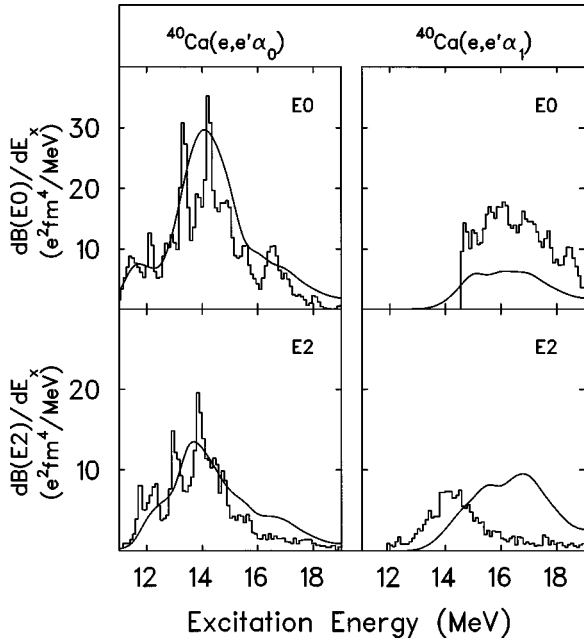


FIG. 6. Experimental $B(E0)$ and $B(E2)$ strength distributions in ^{40}Ca for α_0 and α_1 decay. The solid lines correspond to the calculations of the isoscalar excitation strengths from Ref. [16] multiplied with branching ratios for the decay channels taken from statistical model calculations with the code CASCADE [39].

rather small. Even for the most extreme example discussed here cross sections would change by less than 20% and the influence on the EWSR would be even smaller, since the main differences are at lower energies.

In order to convert the measured cross sections into reduced transition strengths, energy-integrated form factors $F_{EJ}(q)$ for the different multiplicities are calculated for each measured momentum transfer according to

$$|F_{EJ}(q)|^2 = \frac{1}{\sigma_{\text{Mott}}(q)} \int_{11 \text{ MeV}}^{19 \text{ MeV}} \frac{d^2\sigma}{d\Omega dE_x}(q, E_x) dE_x. \quad (6)$$

An extrapolation to the photon point $k = E_x/\hbar c$ is achieved by a fit of theoretical form factors to the experimental values. The form factors are obtained from transition densities calculated in the approach of [16,34] which has been demonstrated to allow for a quantitative description of the GMR and GQR in ^{40}Ca . The transition strength is related to the form factor at the photon point by

$$B(EJ) = \frac{[(2J+1)!!]}{k^{2J}} \frac{Z^2}{4\pi} |F(EJ, q=k)|^2. \quad (7)$$

The distribution of transition strength as a function of excitation energy is then obtained as an error-weighted mean of all measured momentum transfers

$$\frac{dB(EJ)}{dE_x} = \frac{B(EJ)}{|F_{EJ}(q)|^2} \frac{1}{\sigma_{\text{Mott}}(q)} \frac{d^2\sigma}{d\Omega dE_x}(q, E_x), \quad (8)$$

combining Eqs. (6) and (7). The resulting $B(E0)$ and $B(E2)$ distributions are depicted in Fig. 6 for the α_0 and the α_1 channel, respectively. The exhaustion of the EWSR summed

over both channels amounts to 19.8(4.0)% and 11.0(2.2)% for the isoscalar GMR and GQR, respectively.

IV. DISCUSSION

A special feature of the GQR and GMR in ^{40}Ca , which is also found in *fp*-shell nuclei, is a large concentration of reduced transition strength at energies below $E_x < 15$ MeV [28,33,40,41]. This observation is in sharp contrast to RPA theory, which predicts only one strong peak around 18 MeV for both multiplicities [42,43], but can be explained by advanced calculations including the continuum and complex configurations beyond 1p-1h of the 1p-1h \otimes phonon type [16]. As demonstrated in [34], such calculations very satisfactorily account for the strong fragmentation of the isoscalar $E0$ and $E2$ strengths, and a quantitative description of their sum experimentally extracted with a multipole decomposition of 4π -integrated $(e, e'x)$ spectra [28] could be achieved. Here, we present a more detailed comparison of the resolved $E0$ and $E2$ parts for the investigated α decay channels.

The calculated strength distributions are taken from Ref. [16]. There is little difference for $E2$ compared to the previous calculation within the same approach reported in [34], but the $E0$ results are considerably modified [44] by variations of single-particle energies in an attempt to optimize the reproduction of the new GMR data shown in [15]. Because electroexcitation of isovector strength is suppressed in the α channels as discussed above, the theoretical results for the isoscalar response rather than for the total electromagnetic strength are compared to the data. The branching ratio into the final states as a function of ^{40}Ca excitation energy is determined by statistical model calculations with the code CASCADE [39] modified to allow for a proper treatment of isospin [45].

The solid lines in Fig. 6 display the resulting $B(E0)$ and $B(E2)$ distributions for decay into the α_0 and α_1 channels. Very satisfying agreement is found for the GMR and GQR strength decaying to the g.s. of ^{36}Ar . However, while the energy dependence of the $E0$ part in the α_1 channel is reasonably accounted for, the total $B(E0)$ strength is grossly underestimated by a factor of 2.5. The $E2$ contribution in the α_1 channel is only poorly described with a shift of the maximum of about 3 MeV with respect to experiment. This deficiency is largely independent from the phase problem in the analysis of the α_1 decay discussed the previous section, where the main effect would be around $E_x \approx 14-15$ MeV, but little additional $E2$ strength would be added at higher energies. The excess of experimental $B(E2)$ strength around 14 MeV may result from nonstatistical decay contributions. These have been shown to play a role in lighter $N=Z$ nuclei [46]. However, this does not offer an explanation for the underestimate of the $E0$ and overestimate of the $E2$ parts in the α_1 decay by the calculations.

The $B(E0)$ strength distribution from the electron-scattering experiment shown in the upper part of Fig. 7 is compared to the (α, α') results of Ref. [15], middle part, and Ref. [40], lower part. For excitation energies up to 15 MeV, the main structures agree quite well with the data of Ref. [40], although the latter data show a small systematic upward shift of about 100 keV. The comparison with the results of Youngblood *et al.* [15] is less clear. At energies

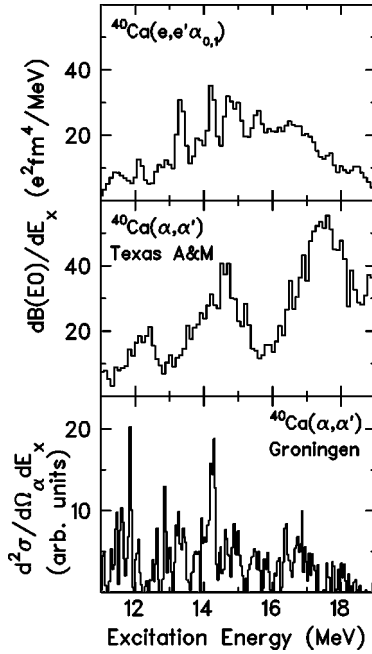


FIG. 7. Top: GMR strength in ^{40}Ca from the present ($e, e' \alpha$) experiment. The histogram represents the summed strengths of the excitation corresponding to decay into the α_0 and α_1 channels. Middle: GMR strength distribution in ^{40}Ca from the (α, α') experiment of Ref. [15]. Bottom: GMR strength distribution in ^{40}Ca from the (α, α') experiment of Ref. [40].

around 12 MeV the agreement of the distributions is not too good, while the gross structure of the bump visible at $E_x \approx 14-16$ corresponds to the electron-scattering results which, however, display more pronounced fine structure. At excitation energies $E_x > 16$ MeV contributions from the α decay to higher-lying states in ^{36}Ar become increasingly important leading to the decrease of $B(E0)$ strength visible in Fig. 7 extracted from the $(e, e' \alpha_{0,1})$ results. (The large difference at higher E_x between the two α -scattering experiments is discussed in detail in [15].)

In order to extract the total EWSR strength from the $(e, e' \alpha_{0,1})$ data, we assume a statistical decay of the GMR which allows for a correction of the nonobserved $E0$ strength due to proton and neutron decay or α decay into higher-lying states. This correction factor was taken from the CASCADE calculations described above. An exhaustion of 44.2(8.8)% is extracted for the isoscalar $E0$ EWSR in the energy range $E_x = 11-19$ MeV from electron scattering using the $\alpha_{0,1}$ statistical model branching ratios, thus roughly doubling the values for the summed $^{40}\text{Ca}(e, e' \alpha_{0,1})$ reactions given in Sec. III. The result may be compared to 33.9(5.5)% for the same energy interval obtained in Ref. [15]. A number of uncertainties enter into the extraction of these numbers. For the $(e, e' \alpha)$ data it is dominated by the described model assumptions, while for the (α, α') data one has to deal with strong background from different reaction types and the general model dependence of the conversion of cross section into transition strength which can have drastic effects (for a recent example in ^{40}Ca , see [47]). With this in mind the agreement between both experiments can be regarded as reasonably good. An EWSR value of 30(6)% in an energy region $E_x = 10.5-20$ MeV is given for the data of Ref. [40].

This number seems surprisingly large considering the strong drop of the cross sections in Fig. 7 above 15 MeV.

The GMR energy centroid E_0 cannot be determined unambiguously from the present data because of the missing information at higher energies. However, if one adopts the $B(E0)$ distribution measured by Youngblood *et al.* [15] for the energy region $E_x > 19$ MeV, a value $E_0 \approx 17.5(1.0)$ MeV is suggested. This would be in slightly better agreement with the prediction of Blaizot *et al.* [6] of $E_0 = 16.2$ MeV based on a compressibility $K_{\text{nm}} \approx 210$ MeV. Such a result would also be in favor of the interaction NL1 (corresponding again to $K_{\text{nm}} \approx 210$ MeV) in the relativistic mean-field calculations [10,11] rather than the higher values $K_{\text{nm}} = 250-270$ favored by them from the comparison to heavier nuclei. Finally, it is noted that the extracted energy centroid would also reasonably agree with the calculations of Kamerdzhev *et al.* [16] which yield $E_0 = 18.4$ MeV.

V. CONCLUSIONS

We have reported a study of the electroinduced α decay in ^{40}Ca from the giant resonance region. The momentum transfer range of $q \approx 0.25-0.66 \text{ fm}^{-1}$ allowed for a simultaneous excitation of the GMR, GDR, and GQR. It was possible to separate the excitations corresponding to the decay into the g.s. ($J^\pi = 0^+$) and first excited state ($J^\pi = 2^+$) of ^{36}Ar and detailed angular correlations have been measured covering angles $\theta_\alpha = 0^\circ-230^\circ$ relative to the momentum transfer axis. It was shown that the formalism [32] developed for a decomposition of $E0$, $E1$, and $E2$ strengths from measured $(e, e' \alpha)$ angular correlations populating a $J^\pi = 0^+$ g.s. in the daughter nucleus can be extended to the decay into a $J^\pi = 2^+$ final state under two assumptions: the cross section ratio of different allowed decay angular momenta for a specific multipole is determined by the transmission coefficients and the relative phase difference between amplitudes for a given resonance J , but neighboring decay angular momenta L , is 180° .

The multipole unfolding of the α_0 and α_1 channels showed a dominance of $E0$ and $E2$ strengths and little $E1$ contributions. Because of isospin selection rules the monopole and quadrupole strength is of isoscalar nature. The resulting $E0$ and $E2$ strength distributions in an excitation energy range $E_x = 11-19$ MeV were compared to the microscopic calculations for the GMR and GQR of Kamerdzhev *et al.* [16] by weighting with statistical model branching ratios. Impressive agreement is observed for the α_0 channel, but the $E0$ strength is underestimated in the α_1 channel, while the calculation of the $E2$ part shows a shift of the maximum by several MeV with respect to the data.

Assuming statistical decay the isoscalar $E0$ EWSR strength was reconstructed from the electron-scattering data. An EWSR exhaustion of 44.2(8.8)% is obtained for the GMR, somewhat larger than what is found with α scattering. Systematic uncertainties have to be considered in both experiments, dominated in the case of electron scattering by the assumption of completely statistical decay, and for hadron scattering experiments by the model dependence of the strength extraction. The present results provide a further example that only a fraction of the isoscalar GMR is found in medium-mass nuclei at energies below 20 MeV. Adopting

the $E0$ strength distribution of Ref. [15] for energies $E_x > 19$ MeV a centroid energy $E_0 \approx 17.5(1.0)$ MeV of the GMR could be extracted. Good agreement with recent microscopic studies is obtained for interactions with a nuclear matter compression modulus $K_{\text{nm}} \approx 210$ MeV.

Further investigations of the GMR in a variety of nuclei with $(e, e'x)$ experiments are clearly of interest for a number of reasons. For example, in Ref. [14] a (α, α') study of ^{58}Ni with the same experimental techniques as reported for ^{40}Ca [15] has revealed only a fraction of at most 50% of the $E0$ EWSR up to an excitation energy as high as 25 MeV. This finding represents a puzzle which might be addressed in an electron-scattering coincidence experiment, since the α decay branching ratios should still be large enough for a meaningful analysis along the ways described here.

Furthermore, electron-scattering coincidence experiments might provide a new access to resolve the strong model dependencies of the conversion of cross sections to transition strengths inherent to hadron-induced experiments as discussed, e.g., in [18,19] for α scattering. In lighter nuclei $E0$ strength distributions and EWSR exhaustions derived from $(e, e' \alpha_0)$ experiments could serve as benchmarks for corresponding $(\alpha, \alpha' \alpha_0)$ measurements. In heavier nuclei, where the GMR and GQR are energetically well separated, the information can be gained in $(e, e'n)$ experiments from the multipole decomposition of 4π -integrated spectra (see, e.g., [22] for an example). Such an experimental setup for $(e, e'n)$ measurements has recently been installed at the S-DALINAC accelerator and first experiments have been performed on ^{48}Ca with very promising results [48].

ACKNOWLEDGMENTS

Discussions with U. Garg, M. N. Harakeh, S. Kamezdzhiev, J. Speth, and A. van der Woude are gratefully acknowledged. We are indebted to D. H. Youngblood for providing us with detailed informations about his experimental results. This work was supported by the Deutsche Forschungsgemeinschaft under Contract No. Ri 242/12-1.

APPENDIX: DETERMINATION OF $E0$, $E1$, AND $E2$ STRENGTH CONTRIBUTIONS AND RELATIVE PHASES FROM $(e, e' \alpha)$ ANGULAR CORRELATION COEFFICIENTS

The coefficients A'_l from Eq. (3) contain the information of angular momentum coupling and account for selection rules. They are given by

$$A'_l(S; LJ; L' J') = [l]^2 [J] [J'] [L] [L'] (-1)^S \begin{Bmatrix} J & J' & l \\ L' & L & S \end{Bmatrix} \\ \times \begin{pmatrix} L & L' & l \\ 0 & 0 & 0 \end{pmatrix} \begin{pmatrix} J & J' & l \\ 0 & 0 & 0 \end{pmatrix} \\ \times \frac{1}{2} [1 + (-1)^l \pi_J \pi_{J'}] \frac{1}{2} [1 + (-1)^{L+J}] \\ \times \frac{1}{2} [1 + (-1)^{L'+J'}], \quad (\text{A1})$$

with $[j] = \sqrt{2j+1}$. The expressions with the round and curly brackets are Wigner $3j$ and $6j$ symbols, respectively. The quantity

$$C_{LJ}^{(S)} e^{i\delta_{LJ}^{(S)}} = (-i)^J \langle LS | J \rangle \frac{(\Gamma_{J/2\pi})^{1/2}}{\omega - \omega_J + i(\Gamma_{J/2})} \langle J || \hat{M}_J || 0 \rangle \quad (\text{A2})$$

is the product between the longitudinal matrix element and the overlap of the intermediate resonance J and the decay channel (LS) . In contrast to the definitions in [36] the amplitudes defined in Eq. (A2) are multiplied with $[J] = \sqrt{2J+1}$, while the coefficients in Eq. (A1) are divided by the factor $[J][J']$.

1. α_0 channel

From the multipole expansion by Legendre polynomials [Eq. (2)] up to $l=4$ one obtains an equation system by evaluating Eq. (3) which relates the angular correlation coefficients A_l to the amplitudes C_{LJ} and phases δ_{LJ} , respectively. For the α_0 channel ($S=0, L=J$) the system of equations becomes

$$A_0 = C_0^2 + C_1^2 + C_2^2, \\ A_1 = \kappa_1 C_0 C_1 \cos \delta^{10} + \kappa_2 C_1 C_2 \cos(\delta^{20} - \delta^{10}), \\ A_2 = \kappa_3 C_1^2 + \kappa_4 C_2^2 + \kappa_5 C_0 C_2 \cos \delta^{20}, \quad (\text{A3}) \\ A_3 = \kappa_6 C_1 C_2 \cos(\delta^{20} - \delta^{10}), \\ A_4 = \kappa_7 C_2^2,$$

with $\delta^{10} \equiv \delta_1 - \delta_0$ and $\delta^{20} \equiv \delta_2 - \delta_0$. The constant factors κ_i are given by $\kappa_1 = 2\sqrt{3}$, $\kappa_2 = \frac{4}{5}\sqrt{15}$, $\kappa_3 = 2$, $\kappa_4 = 10/7$, $\kappa_5 = 2\sqrt{5}$, $\kappa_6 = \frac{6}{5}\sqrt{5}$, and $\kappa_7 = 18/7$. Using the abbreviations

$$B_0 = A_0 - \frac{1}{\kappa_7} A_4 = C_0^2 + C_1^2, \\ B_1 = \frac{1}{\kappa_1} A_1 - \frac{\kappa_2}{\kappa_1 \kappa_6} A_3 = C_0 C_1 \cos \delta^{10}, \\ B_2 = \frac{1}{\kappa_3} A_2 - \frac{\kappa_4}{\kappa_3 \kappa_7} A_4 = C_1^2 + \frac{\kappa_5}{\kappa_3} C_0 C_2 \cos \delta^{20}, \quad (\text{A4}) \\ B_3 = \frac{1}{\kappa_6} A_3 = C_1 C_2 \cos(\delta^{20} - \delta^{10}), \\ B_4 = \frac{1}{\kappa_7} A_4 = C_2^2,$$

and

$$k_1 = -3B_0 + 2B_2 - \gamma^2 B_4, \\ k_2 = 3B_0^2 - 4B_0 B_2 + B_2^2 + \gamma^2 B_0 B_4 + 2\gamma B_1 B_3 - \gamma^2 B_3^2, \quad (\text{A5})$$

$$k_3 = -B_0^3 + 2B_0^2B_2 - B_0B_2^2 - \gamma^2B_1^2B_4 + 2\gamma B_1B_2B_3 \quad \text{and} \\ -2\gamma B_0B_1B_3,$$

$$\delta^{20} = \arccos \frac{B_2 - C_1^2}{\gamma C_0 C_2}. \quad (\text{A7})$$

with $\gamma \equiv \kappa_5 / \kappa_3$, one obtains C_0^2 by solving the cubic equation

$$C_0^6 + k_1 C_0^4 + k_2 C_0^2 + k_3 = 0. \quad (\text{A6})$$

The remaining unknown quantities are determined by

$$C_1^2 = B_0 - C_0^2, \quad C_2^2 = B_4, \quad \delta^{10} = \arccos \frac{B_1}{C_0 C_1},$$

While the equation system Eq. (A3) provides unique results for the highest multipolarity ($J=2$), there are generally three solutions of Eq. (A6). The criteria to identify the physically correct solution have been discussed in Sec. III.

2. α_1 channel

For the α_1 channel, the equation system for the A_l 's is given by

$$A_0 = C_{20}^2 + C_{11}^2 + C_{13}^2 + C_{02}^2 + C_{22}^2 + C_{42}^2,$$

$$A_1 = -2\sqrt{\frac{6}{5}}C_{20}C_{11}\cos(\delta_{11} - \delta_{20}) + \frac{6}{5}\sqrt{5}C_{20}C_{31}\cos(\delta_{31} - \delta_{20}) - 2\sqrt{\frac{6}{5}}C_{11}C_{02}\cos(\delta_{02} - \delta_{11}) + \frac{6}{5}\sqrt{\frac{7}{3}}C_{11}C_{22}\cos(\delta_{22} - \delta_{11}) \\ - \frac{6}{5}\sqrt{\frac{2}{7}}C_{31}C_{22}\cos(\delta_{22} - \delta_{31}) + 12\sqrt{\frac{2}{35}}C_{31}C_{42}\cos(\delta_{42} - \delta_{31}),$$

$$A_2 = \frac{1}{5}C_{11}^2 - \frac{6}{5}\sqrt{6}C_{11}C_{31}\cos(\delta_{31} - \delta_{11}) + \frac{4}{5}C_{31}^2 - 2\sqrt{\frac{10}{7}}C_{02}C_{22}\cos(\delta_{22} - \delta_{02}) - \frac{15}{49}C_{22}^2 - \frac{24}{49}C_{22}C_{42}\cos(\delta_{42} - \delta_{22}) + \frac{50}{49}C_{42}^2 \\ + 2C_{20}C_{02}\cos(\delta_{02} - \delta_{20}) - 2\sqrt{\frac{10}{7}}C_{20}C_{22}\cos(\delta_{22} - \delta_{20}) + 6\sqrt{\frac{2}{7}}C_{20}C_{42}\cos(\delta_{42} - \delta_{20}), \quad (\text{A8})$$

$$A_3 = \frac{6}{5}\sqrt{\frac{3}{7}}C_{11}C_{22}\cos(\delta_{22} - \delta_{11}) - 12\sqrt{\frac{3}{35}}C_{11}C_{42}\cos(\delta_{42} - \delta_{11}) + \frac{6}{5}\sqrt{5}C_{31}C_{02}\cos(\delta_{02} - \delta_{31}) - \frac{24}{5}\sqrt{\frac{2}{7}}C_{31}C_{22}\cos(\delta_{22} - \delta_{31}) \\ + 6\sqrt{\frac{2}{35}}C_{31}C_{42}\cos(\delta_{42} - \delta_{31}),$$

$$A_4 = 6\sqrt{\frac{2}{7}}C_{02}C_{42}\cos(\delta_{42} - \delta_{02}) + \frac{36}{49}C_{22}^2 - \frac{60}{49}\sqrt{5}C_{22}C_{42}\cos(\delta_{42} - \delta_{22}) + \frac{27}{7}C_{42}^2.$$

After introduction of the branchings β_L describing the weights of the possible L channels [Eq. (4)] corresponding to the decay of a resonance with spin J , three unknown amplitudes can be removed from the equation system (A8) and one obtains

$$A_0 = C_0^2 + C_1^2 + C_2^2,$$

$$A_1 = \left[-2\sqrt{\frac{6}{5}}\sqrt{\beta_1}\cos(\delta_{11} - \delta_{20}) + \frac{6}{5}\sqrt{5}\sqrt{\beta_3}\cos(\delta_{31} - \delta_{20}) \right] C_0 C_1 + \left[-2\sqrt{\frac{6}{5}}\sqrt{\beta_0\beta_1}\cos(\delta_{02} - \delta_{11}) \right. \\ \left. + \frac{6}{5}\sqrt{\frac{7}{3}}\sqrt{\beta_1\beta_2}\cos(\delta_{22} - \delta_{11}) - \frac{6}{5}\sqrt{\frac{2}{7}}\sqrt{\beta_2\beta_3}\cos(\delta_{22} - \delta_{31}) + \frac{12}{5}\sqrt{\frac{10}{7}}\sqrt{\beta_3\beta_4}\cos(\delta_{42} - \delta_{31}) \right] C_1 C_2,$$

$$A_2 = \left[\frac{1}{5}\beta_1 - \frac{6}{5}\sqrt{6}\sqrt{\beta_1\beta_3}\cos(\delta_{31} - \delta_{11}) + \frac{4}{5}\beta_3 \right] C_1^2 + \left[-2\sqrt{\frac{10}{7}}\sqrt{\beta_0\beta_2}\cos(\delta_{22} - \delta_{02}) - \frac{24}{49}\sqrt{\beta_2\beta_4}\cos(\delta_{42} - \delta_{22}) \right. \\ \left. - \frac{15}{49}\beta_2 + \frac{50}{49}\beta_4 \right] C_2^2 + \left[2\sqrt{\beta_0}\cos(\delta_{02} - \delta_{20}) - 2\sqrt{\frac{10}{7}}\sqrt{\beta_2}\cos(\delta_{22} - \delta_{20}) + 6\sqrt{\frac{2}{7}}\sqrt{\beta_4}\cos(\delta_{42} - \delta_{20}) \right] C_0 C_2, \quad (\text{A9})$$

$$A_3 = \left[\frac{6}{5} \sqrt{\frac{3}{7}} \sqrt{\beta_1 \beta_2} \cos(\delta_{22} - \delta_{11}) - \frac{12}{5} \sqrt{\frac{15}{7}} \sqrt{\beta_1 \beta_4} \cos(\delta_{42} - \delta_{11}) + \frac{6}{5} \sqrt{5} \sqrt{\beta_0 \beta_3} \cos(\delta_{02} - \delta_{31}) - \frac{24}{5} \sqrt{\frac{2}{7}} \sqrt{\beta_2 \beta_3} \cos(\delta_{22} - \delta_{31}) \right. \\ \left. + \frac{6}{5} \sqrt{\frac{10}{7}} \sqrt{\beta_3 \beta_4} \cos(\delta_{42} - \delta_{31}) \right] C_1 C_2, \\ A_4 = \left[6 \sqrt{\frac{2}{7}} \sqrt{\beta_0 \beta_4} \cos(\delta_{42} - \delta_{02}) + \frac{36}{49} \beta_2 - \frac{60}{49} \sqrt{5} \sqrt{\beta_2 \beta_4} \cos(\delta_{42} - \delta_{22}) + \frac{27}{7} \beta_4 \right] C_2^2.$$

Two extreme cases are possible for the phase difference $e^{i(\delta_{L'} - \delta_{L'})}$. For a choice of 0° one finds no physically possible solution for the whole investigated excitation energy range, i.e., at least one of the squared amplitudes C_j^2 always becomes negative. With the assumption $e^{i(\delta_{L'} - \delta_{L'})} = i^{(L-L')}$ and $\delta_0 \equiv \delta_{20}$, $\delta_1 \equiv \delta_{11}$, $\delta_2 \equiv \delta_{02}$ one obtains an equation system with the same structure as Eqs. (A3). The coefficients κ_i are given for the α_1 channel by

$$\kappa_1 = -2 \sqrt{\frac{6}{5}} \sqrt{\beta_1} - \frac{6}{5} \sqrt{5} \sqrt{\beta_3}, \\ \kappa_2 = -2 \sqrt{\frac{6}{5}} \sqrt{\beta_0 \beta_1} - \frac{6}{5} \sqrt{\frac{7}{3}} \sqrt{\beta_1 \beta_2} - \frac{6}{5} \sqrt{\frac{2}{7}} \sqrt{\beta_2 \beta_3} - 12 \sqrt{\frac{2}{35}} \sqrt{\beta_3 \beta_4}, \\ \kappa_3 = \frac{1}{5} \beta_1 + \frac{6}{5} \sqrt{6} \sqrt{\beta_1 \beta_3} + \frac{4}{5} \beta_3, \\ \kappa_4 = 2 \sqrt{\frac{10}{7}} \sqrt{\beta_0 \beta_2} - \frac{15}{49} \beta_2 + \frac{24}{49} \sqrt{\beta_2 \beta_4} + \frac{50}{49} \beta_4, \\ \kappa_5 = 2 \sqrt{\beta_0} + 2 \sqrt{\frac{10}{7}} \sqrt{\beta_2} + 6 \sqrt{\frac{2}{7}} \sqrt{\beta_4}, \\ \kappa_6 = -\frac{6}{5} \sqrt{\frac{3}{7}} \sqrt{\beta_1 \beta_2} - 12 \sqrt{\frac{3}{35}} \sqrt{\beta_1 \beta_4} - \frac{6}{5} \sqrt{5} \sqrt{\beta_0 \beta_3} - \frac{24}{5} \sqrt{\frac{2}{7}} \sqrt{\beta_2 \beta_3} - 6 \sqrt{\frac{2}{35}} \sqrt{\beta_3 \beta_4}, \\ \kappa_7 = 6 \sqrt{\frac{2}{7}} \sqrt{\beta_0 \beta_4} + \frac{36}{49} \beta_2 + \frac{60}{49} \sqrt{5} \sqrt{\beta_2 \beta_4} + \frac{27}{7} \beta_4. \tag{A10}$$

In contrast to the α_0 channel, the κ_i contain the weights of the L channels β_L and are thus dependent on excitation energy. The factors κ_1 , κ_2 , and κ_6 change their signs with respect to the α_0 channel, and therefore also A_1 and A_3 . Such a phase inversion between the α_0 and the α_1 channel reflects itself in the relative ratio of the angular correlations at 0° and 180° and is indeed visible in the data. The solutions for the remaining variables are again given by Eqs. (A4)–(A7).

-
- [1] J. P. Blaizot, *Phys. Rep.* **64**, 171 (1980).
[2] A. van der Woude, in *Electric and Magnetic Giant Resonances in Nuclei*, edited by J. Speth (World Scientific, Singapore, 1991), p. 100.
[3] Y. W. Lui, J. D. Bronson, D. H. Youngblood, Y. Toba, and U. Garg, *Phys. Rev. C* **31**, 1643 (1985).
[4] H. J. Lu, S. Brandenburg, R. de Leo, A. G. Drentje, M. N. Harakeh, H. Sakai, and A. van der Woude, *Phys. Rev. C* **33**, 1116 (1986).
[5] J. Treiner, H. Krivine, O. Bohigas, and J. Martorell, *Nucl. Phys.* **A371**, 253 (1981).
[6] J. P. Blaizot, J. F. Berger, J. Dechargé, and M. Girod, *Nucl. Phys.* **A591**, 435 (1995).
[7] M. M. Sharma, W. T. A. Borghols, S. Brandenburg, S. Crona, A. van der Woude, and M. N. Harakeh, *Phys. Rev. C* **38**, 2562 (1988).
[8] J. M. Pearson, *Phys. Lett. B* **271**, 12 (1991).
[9] S. Shlomo and D. H. Youngblood, *Phys. Rev. C* **47**, 529 (1993).
[10] M. V. Stoitsov, P. Ring, and M. M. Sharma, *Phys. Rev. C* **50**, 1445 (1994).
[11] D. Vretenar, G. A. Lalazissis, B. Behnsch, W. Pöschl, and P. Ring, *Nucl. Phys.* **A621**, 853 (1997).
[12] C. S. Wang, K. C. Ching, and A. J. Santiago, *Phys. Rev. C* **55**, 2844 (1997).
[13] I. Hamamoto, H. Sagawa, and X. Z. Zhang, *Phys. Rev. C* **56**, 3121 (1997).
[14] D. H. Youngblood, H. L. Clark, and Y.-W. Lui, *Phys. Rev. Lett.* **76**, 1429 (1996).

- [15] D. H. Youngblood, H. L. Clark, and Y.-W. Lui, *Phys. Rev. C* **55**, 2811 (1997).
- [16] S. Kamezdzhiev, J. Speth, and G. Tertychny, *Nucl. Phys.* **A624**, 328 (1997).
- [17] G. R. Satchler, *Nucl. Phys.* **A472**, 215 (1987).
- [18] G. R. Satchler and D. T. Khoa, *Phys. Rev. C* **55**, 285 (1997).
- [19] D. H. Youngblood, *Phys. Rev. C* **55**, 950 (1997).
- [20] J. R. Calarco, J. Arruda-Neto, K. A. Griffioen, S. S. Hanna, D. H. Hoffmann, B. Neyer, R. E. Rand, K. Wienhard, and M. R. Yearian, *Phys. Lett.* **146B**, 179 (1984).
- [21] T. Kihm, K. T. Knöpfle, H. Riedesel, P. Voruganti, H. J. Emrich, G. Fricke, R. Neuhausen, and R. K. M. Schneider, *Phys. Rev. Lett.* **56**, 2789 (1986).
- [22] G. O. Bolme, L. S. Cardman, R. Doerfler, L. J. Koester, Jr., B. L. Miller, C. N. Papanicolas, H. Rothhaas, and S. E. Williamson, *Phys. Rev. Lett.* **61**, 1081 (1988).
- [23] A. Tanaka, T. Hino, H. Kawahara, N. Nomura, T. Tamae, M. Sugawara, H. Tsubota, H. Miyase, and Y. Kawazoe, *Nucl. Phys.* **A489**, 381 (1988).
- [24] R. A. Miskimen, E. A. Ammons, J. D. T. Arruda-Neto, L. S. Cardman, P. L. Cole, J. R. Deininger, S. M. Dolfini, A. J. Linzey, J. B. Mandeville, B. L. Miller, P. E. Mueller, C. N. Papanicolas, A. Serdarevič, and S. E. Williamson, *Phys. Lett. B* **236**, 251 (1990); *Phys. Rev. C* **43**, 1677 (1991).
- [25] J. P. Fritsch, H. J. Emrich, A. Grasmück, R. Neuhausen, S. Schardt, N. Zimmermann, J. R. Calarco, and M. Potokar, *Phys. Rev. Lett.* **68**, 1667 (1992).
- [26] J. DeAngelis, J. R. Calarco, J. E. Wise, H. J. Emrich, R. Neuhausen, and H. Weyand, *Phys. Rev. Lett.* **70**, 2872 (1993); *Phys. Rev. C* **52**, 61 (1995).
- [27] L. A. A. Terremeto, V. P. Likachev, M. N. Martins, H. J. Emrich, G. Fricke, T. Kröhl, and K. W. Neff, *Phys. Rev. C* **56**, 2597 (1997).
- [28] H. Diesener, U. Helm, G. Herbert, V. Huck, P. von Neumann-Cosel, C. Rangacharyulu, A. Richter, G. Schrieder, A. Stascheck, A. Stiller, J. Ryckebusch, and J. Carter, *Phys. Rev. Lett.* **72**, 1994 (1994).
- [29] T. Saito, S. Suzuki, T. Takahisa, C. Takakuwa, M. Oikawa, T. Tohei, T. Nakagawa, and K. Abe, *Phys. Rev. Lett.* **78**, 1018 (1997).
- [30] P. von Neumann-Cosel, C. Rangacharyulu, A. Richter, G. Schrieder, A. Stascheck, and S. Strauch, *Phys. Rev. Lett.* **78**, 2924 (1997).
- [31] P. von Neumann-Cosel, H. Diesener, U. Helm, G. Herbert, V. Huck, C. Rangacharyulu, A. Richter, G. Schrieder, A. Stascheck, A. Stiller, J. Ryckebusch, J. Carter, A. A. Cowley, R. W. Fearick, J. J. Lawrie, S. J. Mills, R. T. Newman, J. V. Pilcher, F. D. Smit, Z. Z. Vilakazi, and D. M. Whittal, *Nucl. Phys.* **A569**, 373c (1994).
- [32] M. Spahn, T. Kihm, and K. T. Knöpfle, *Z. Phys. A* **330**, 345 (1988).
- [33] H. Diesener, U. Helm, P. von Neumann-Cosel, A. Richter, G. Schrieder, and S. Strauch, *Phys. Lett. B* **352**, 201 (1995).
- [34] S. Kamezdzhiev, J. Speth, and G. Tertychny, *Phys. Rev. Lett.* **74**, 3943 (1995).
- [35] H. Ehrenberg, M. Averdung, B. Dreher, G. Fricke, H. Herminghaus, R. Herr, H. Hultsch, G. Lührs, K. Mehrle, R. Neuhausen, G. Nöldeke, H. M. Stoltz, V. Walther, and H. D. Wohlfahrt, *Nucl. Instrum. Methods* **105**, 253 (1972).
- [36] W. E. Kleppinger and J. D. Walecka, *Ann. Phys. (N.Y.)* **146**, 349 (1983).
- [37] U. Helm, Ph.D. thesis D17, Technische Hochschule Darmstadt, 1990.
- [38] H. Diesener, Ph.D. thesis D17, Technische Hochschule Darmstadt, 1995.
- [39] F. Pühlhofer, *Nucl. Phys.* **A280**, 267 (1977).
- [40] S. Brandenburg, R. de Leo, A. G. Drentje, M. N. Harakeh, H. Sakai, and A. van der Woude, *Phys. Lett.* **130B**, 9 (1983).
- [41] F. Zwarts, A. G. Drentje, M. N. Harakeh, and A. van der Woude, *Phys. Lett.* **125B**, 123 (1983); *Nucl. Phys.* **A439**, 117 (1985).
- [42] P. F. Bortignon and R. A. Broglia, *Nucl. Phys.* **A381**, 405 (1981).
- [43] S. Drożdż, V. Klemt, J. Speth, and J. Wambach, *Nucl. Phys.* **A451**, 11 (1986).
- [44] S. Kamezdzhiev, J. Speth, G. Tertychny, and J. Wambach, *Nucl. Phys.* **A577**, 641 (1994).
- [45] M. N. Harakeh (private communication).
- [46] K. T. Knöpfle and G. J. Wagner, in *Electric and Magnetic Giant Resonances in Nuclei* [2], p. 234.
- [47] J. Carter, A. A. Cowley, H. Diesener, R. W. Fearick, S. V. Förtsch, M. N. Harakeh, J. J. Lawrie, S. J. Mills, P. von Neumann-Cosel, R. T. Newman, J. V. Pilcher, A. Richter, K. Schweda, F. D. Smit, G. F. Steyn, S. Strauch, and D. M. Whittal, *Nucl. Phys. A* (in press).
- [48] S. Strauch, Ph.D. thesis D17, Technische Universität Darmstadt, 1998.